J. Shanghai Jiao Tong Univ. (Sci.), 2023
https://doi.org/10.1007/s12204-023-2650-7

Static and Fatigue Behavior of Hybrid Bonded/Bolted Glass Fiber Reinforced Polymer Joints Under Tensile Loading

WANG Jinxiao[1] (王进潇), *CHENG Bin*[1,2,3*] (程 斌), *XIANG Sheng*[1] (向 升), *LI Sida*[1] (李思达), *YAN Xingfei*[4] (闫兴非)
(1. Department of Civil Engineering, Shanghai Jiao Tong University, Shanghai 200240, China; 2. Shanghai Key Laboratory for Digital Maintenance of Buildings and Infrastructure, Shanghai 200240, China; 3. State Key Laboratory of Ocean Engineering, Shanghai 200240, China; 4. Shanghai Urban Construction Design and Research Institute (Group) Co., Ltd., Shanghai 200125, China)

Abstract: This paper presents the static and fatigue tests of hybrid (bonded/bolted) glass fiber reinforced polymer (GFRP) joints. Nine specimens of single-lap hybrid GFRP joints have been fabricated to study the static and fatigue behaviors in the experimental campaign. The static tests of uniaxial tension loading are first conducted, from which the static ultimate bearing capacities of the joints are obtained. High-cycle fatigue tests are subsequently carried out so that the fatigue failure mode, fatigue life, and stiffness degradation of joints can be obtained. The measuring techniques including acoustic emission monitoring and three-dimensional digital image correlation have been employed in the tests to record the damage development process. The results revealed that the static strength and fatigue behavior of such thick hybrid GFRP joints were controlled by the bolted connections. The four stages of fatigue failure process are obtained from tests and acoustic emission signals analysis: cumulative damage of adhesive layer, damage of the adhesive layer, cumulative damage of GFRP plate, and damage of GFRP plate. The fatigue life and stiffness degradation can be improved by more bolts. The *S*-*N* (fatigue stress versus life) curves for the fatigue design of the single-lap hybrid GFRP joints under uniaxial tension loading are also proposed.

Key words: glass fiber reinforced polymer (GFRP) joint, hybrid bonded/bolted connection, fatigue behavior, acoustic emission, digital image correlation
CLC number: TU 399 **Document code:** A

0 Introduction

Fiber reinforced polymer (FRP) has been a type of new material with a rapid development in the past few years in the field of civil engineering, owing to its advantages of lightweight, high strength, and good corrosion resistance. Compared to the conventional concrete and steel structures, the FRP structures can achieve a prior mechanical property; however, their application is impeded by the connecting techniques between FRP plates, which remains an important issue to be further solved. The FRP plates or components in the engineering structures are mainly connected with the types of the bonded, bolted, and hybrid solutions (i.e., combining bonded and bolted)[1]. The bonded connection has the advantages of no drilling and the convenience in construction; however, the bonding strength in this type of connection was found to be discrete due to the defects formed in the construction stage. The bolted connection commonly has relatively high bearing capacity and reliability, while the bolt holes may cause the local damages of FRP material near the holes and thus reduce the overall strength of the joint. The concept of hybrid joint combines the advantages of both bonded and bolted connections, which is thought to be a promising solution for the connections in the FRP structures.

In recent years, numerous studies have been performed by researchers to investigate the mechanical properties of the FRP bolted joints. McCarthy et al.[2-3] studied the influence of bolt clearance on the strength and stiffness of bolted carbon fiber reinforced polymer (CFRP) joints, from which it was found that bolt clearance has limited effect on the joint strength while the joint stiffness would decrease with the increase of the clearance. By experimental study, Sun et al.[4-5] found that there is not a clear relationship between the bolt preload and the failure mode of CFRP joint; however,

Received: 2022-08-17 **Accepted:** 2022-09-27
Foundation item: the National Natural Science Foundation of China (No. 51978400)
*__E-mail:__ cheng_bin@sjtu.edu.cn

it was found that the preload has a remarkable impact on the failure strength of joint. By conducting static loading tests, Khashaba et al.[6] and Sen et al.[7] studied the effects of ply sequence, preload and washer size on the mechanical properties of glass fiber reinforced polymer (GFRP) bolted joints. The results indicate that the bearing strength of joints can be improved with increasing the preload, the reduction of washer size would lead to an increase of joint stiffness, and the failure mode of joint is significantly affected by the ply schemes. Iorio et al.[8] conducted an experimental study on the stiffness degradation of double-lap CFRP bolted joints under the cyclic load with constant amplitude, where the slippage between the connected plates was adopted to evaluate the degradation of joint stiffness, and from the results it was found that joint stiffness would decrease sharply when the joints approach to failure. By conducting a fatigue test of FRP bolted joint under tensile loading, Herrington and Sabaghian[9] found that the direction of the outer ply has a limited effect on the fatigue life of CFRP joint, while an increase in the bolt torque would result in an improvement of fatigue life.

Regarding FRP bonded joints, research work has been reported in litareture. A static finite element analysis (FEA) of CFRP bonded joints was conducted by Huang et al.[10], from which it was revealed that the effect of adhesive layer thickness on the joint force is quite insignificant, which even can be neglected. Read and Shenoi[11] studied the stiffness degradation and the residual strength of single-layer GFRP T-shape bonded joints based on a fatigue test of constant loading amplitude, the maximum and minimum deflections increased steadily before failure, and there was a sudden drop at the failure stage. By experimental investigation, Quaresimin and Ricotta[12] carried out a two-dimensional FEA to predict the crack initiation in the composite cemented layer of bonded CFRP joint (1.65 mm) under fatigue loading, and it was found that increasing the lapping length can remarkably improve the fatigue life of joint. The crack propagations of single- and double-lap FRP bonded joints under constant-amplitude fatigue loading have been experimentally investigated by Zhang et al.[13], from which it can be observed that two kinds of GFRP joint cracks were initiated near the edge of adhesive layer. Kim et al.[14] compared the failure modes of single-lap bonded CFRP joints with different fabrication processes, by which it was also found that the initial cracks occurred at the edge of adhesive layer, and there could be a remarkable dispersion for the bearing capacity when the thickness of adhesive was smaller than 0.2 mm.

For the mechanical characteristics of hybrid bonded/bolted FRP joints, several studies have been reported in literature. Sarkani et al.[15] presented a linear damage accumulation model for predicting the fatigue life of GFRP bonded, bolted, and hybrid bonded/bolted joints under constant-amplitude load. The fatigue resistance of CFRP hybrid bonded/bolted joints has been assessed by Kelly[16] and it was found that the bolts can significantly improve the fatigue life of the hybrid CFRP joints. Through finite element simulation, Hoang-Ngoc and Paroissien[17] studied the fatigue bending performance of the single-lap hybrid, from which it was found that the fatigue life of hybrid joints is longer than the fatigue life for corresponding bolted joints. Focusing on the single- and double-lap CFRP hybrid joints, Chowdhury et al.[18-19] investigated the difference among bolted, bonded, and hybrid joints on the fatigue life of CFRP hybrid joints. The fatigue life of the hybrid joint is almost twice that of its corresponding bonded joint, and bolts can delay the initial crack and improve the fatigue life of the joint. By experimental study, Raju et al.[20] compared the bearing capacities of the bonded/bolted hybrid CFRP joints with the interference fit bolts and ordinary bolts, and the result showed that the strength of the improved joint had been increased by 10%. The static test results indicated that the bonded-connection failed with the seperation of adherends, and the bolted-connection failed with the compressive failure of fiber, but the details of damage process and failure mode of fatigue tests were not mentioned.

To sum up, many studies have been conducted to investigate the mechanical properties of FRP joints; however, most of the investigations are limited in the pure bonded or bolted connections with the FRP thin plates of 2—10 mm in thickness[2-20]. Research on hybrid connection was limited, and monitor methods during fatigue loading are still a problem to be conducted. The studies regarding the static and fatigue performance of FRP joints with thick plates (e.g., greater than 10 mm) have rarely been reported. The existing fatigue tests focusing on the hybrid joint mainly adopted a constant-amplitude loading, which is suitable for the joints with relatively thin FRP plates where the strength values of adhesive failure and bolted failure are comparable. For the hybrid joints with relatively thick FRP plates, the difference of the strength between the two stages would be remarkable and thus using the loading scheme with different load amplitudes is beneficial for revealing the damage process in every loading stage. In order to promote the applications of GFRP structures, it is necessary to investigate the fatigue performance of the GFRP hybrid bonded/bolted joints subjected to various loading conditions.

In this study, the fatigue performance and mechanism of the single-lap GFRP joints under tensile loading condition are experimentally investigated via high cyclic fatigue tests. Nine specimens of single-lap GFRP hybrid bonded/bolted joints are fabricated and tested considering different loading amplitudes. Advanced

measuring technologies including the acoustic emission (AE) and three-dimensional digital image correlation (3D-DIC) are adopted to accurately capture the damage process of the test specimens.

1 Specimens

1.1 Fabrication of GFRP Plates

The detailed geometric dimensions of the test specimens are shown in Fig. 1. The test specimens of the single-lap GFRP hybrid bonded/bolted joint are fabricated by two GFRP plates that are relatively thick, which can reflect the joint properties of the actual engineering structures such as all GFRP bridge girders. The geometric sizes of GFRP plates for all the test specimens are identical: 20 mm in thickness, 160 mm in width, and 480 mm in length. All the plates are fabricated by the 600 g/m^2 unidirectional E-glass fiber and the unsaturated polyester resin with vacuum pouring method. The fiber architecture of the fiber ply for the plates is shown in Table 1, noting that the fiber plies are 0° dominated to bear tensile load. The test specimens are labeled as HTY-i, where H represents the hybrid connection, T indicates the tensile loading condition, Y means the number of bolts, and i is the sequence number of the test specimens in each group. Nine specimens in total are prepared in the current study, and they are divided into three groups according to the number of bolts, which are respectively single bolt, four bolts, and nine bolts, as listed in Table 1. The mechanical properties of the fabricated GFRP plates are tested based on the specification GB/T 3354—1999[21], and the relevant values are given in Table 2. Herein, E and G respectively represent the elastic modulus and shear modulus and the subscripts 1 and 2 respectively denote the longitudinal and transverse directions of the fibers; f_x, f_y and τ are respectively the strength of the fibers in the longitudinal, transverse and shear directions, and the subscripts c and t respectively denote the compressive and tensile.

The fabrication of the test specimens is illustrated in Fig. 2. Before fabrication, the raw materials and equipment including the glass mold, glass fiber cloth, guided net, release cloth, guided pipe, vacuum bag, air pump, release agent, and resin are prepared in advance. The test specimens are fabricated through several stages which are as follows:

(1) The release agent is applied on the mold.

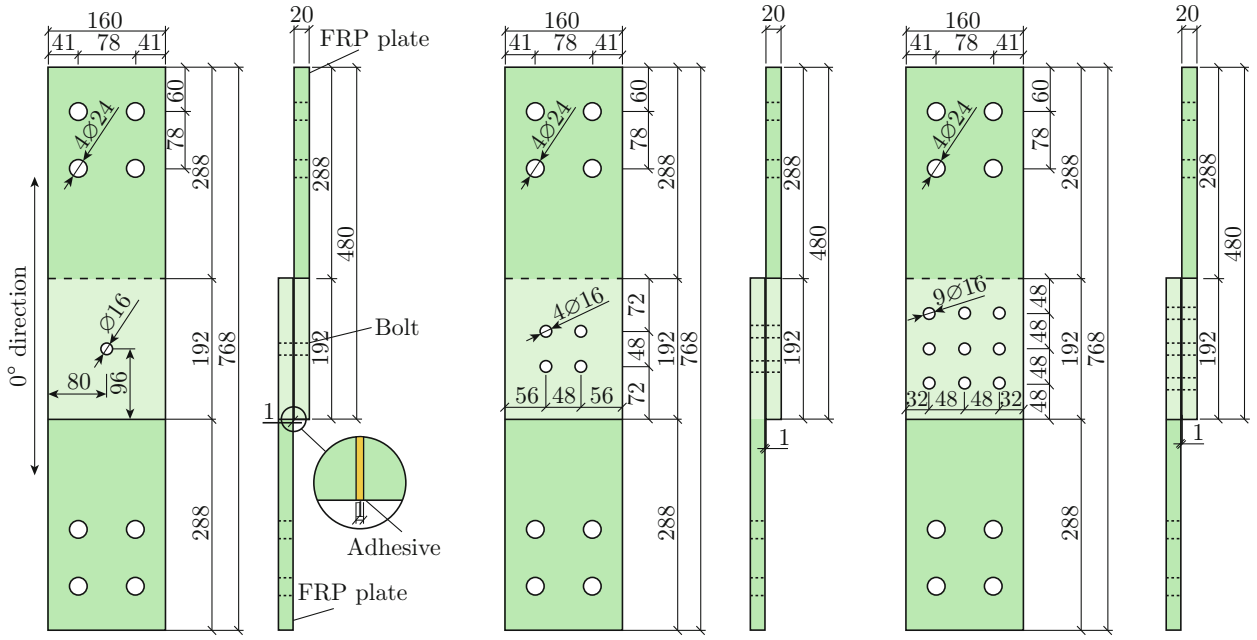

(a) Single-bolt (b) Four-bolt (c) Nine-bolt

Fig. 1 Dimensions of specimens (mm)

Table 1 Dimensions and ply scheme of specimens

Specimen	Number of bolts	Size of GFRP plate/(mm × mm × mm)	Ply scheme	Load
HT1-1	1	480 × 160 × 20	$[(0/0/+45/\text{-}45/90/0/90/0)_2]_S$	Static
HT1-2, HT1-3	1			Fatigue
HT4-1	4			Static
HT4-2, HT4-3	4			Fatigue
HT9-1	9			Static
HT9-2, HT9-3	9			Fatigue

Table 2 Mechanical properties of GFRP

Parameter	Value/GPa	Parameter	Value/MPa
E_{11}	26.8	$f_{x,\mathrm{t}}$	727.31
E_{22}	4.0	$f_{x,\mathrm{c}}$	727.31
G_{12}	4.5	$f_{y,\mathrm{t}}$	70.98
τ_{12}	35	$f_{y,\mathrm{c}}$	142

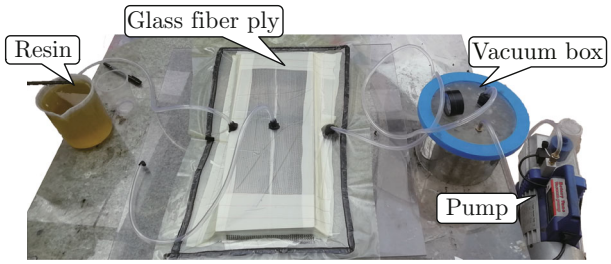

Fig. 2 Fabrication of specimens

(2) The glass fiber cloth, which had been cut into appropriate size by electric scissors, is laid on the bottom mold according to the designed ply scheme.

(3) The spiral guided pipe and injection supports near the inlet and outlet of the mold, the guided net, and the molding cloth are placed.

(4) The top mold is installed above the glass fiber cloth.

(5) The vacuum bag is sealed with sealant, and the conduit is inserted to the vacuum bag, connecting with the vacuum pump. The quality of sealing is thought to be acceptable if the air pressure in the vacuum bag had not changed obviously within 2 min.

(6) The conduit connected to the inlet is inserted into the prepared resin for extraction. Once the resin fills up the vacuum bag and outflows from the outlet conduit, the vacuum pump will be turned off and the conduit will be tightened.

(7) As the resin has been solidified, the mold and the relevant equipment are removed, and then the GFRP plate is cut and perforated according to the designated dimensions of the test specimens.

1.2 Assembly of Joints

To assemble the hybrid GFRP joint specimens, the overlapping surfaces of the GFRP plates are first bonded by using the structural adhesive lica-201 produced by Nanjing Haituo company, and then bolted by the stainless steel outer hexagon bolts A2-70 with a diameter of 16 mm. The material properties of the adhesive and bolts, which are given by the manufacturers, are given in Table 3, where the E and σ represent the elastic modulus and strength of materials, respectively. For each specimen, before bonding the two plates with the structural adhesive, the bonding surfaces are first cleaned up by using acetone in order to optimize the bond quality. Subsequently, steel bolts are applied to bolt the bonded joint before the structural adhesive is cured, tightened with a torque of $20\,\mathrm{N}\cdot\mathrm{m}$. For the final joint specimens, the average thickness of the adhesive layer is measured to be 1 mm. In general, an increase in the tightening torque can improve the resistance of the plate to the eccentric bending moment, while excessive torque would cause the plate damages in the thickness direction[4].

Table 3 Mechanical properties of adhesive and bolts

Bolt (steel)		Adhesive	
Properties	Value	Properties	Value
E_{bolt}/GPa	210	$\sigma_{\mathrm{adhesive}}$/MPa	25
σ_{bolt}/MPa	700	—	—

One of the specimens in each group is tested under static loading to obtain the static strength, while the other two specimens are expected to be tested under cyclic loading for the investigation of fatigue performance. The specimen number, dimension, load condition, and fiber ply scheme of the test specimens are presented in Table 1.

2 Experimental Setup

2.1 Test Rig

The tensile test in the study is carried out on the structural fatigue loading system IST PL-630 in the Test Center of Civil Engineering at Shanghai Jiao Tong University. As illustrated in Fig. 3, the upper clamp of the loading system is directly connected with the fatigue actuator, and the lower clamp is fixed to a bottom girder. The test specimen locates between the upper

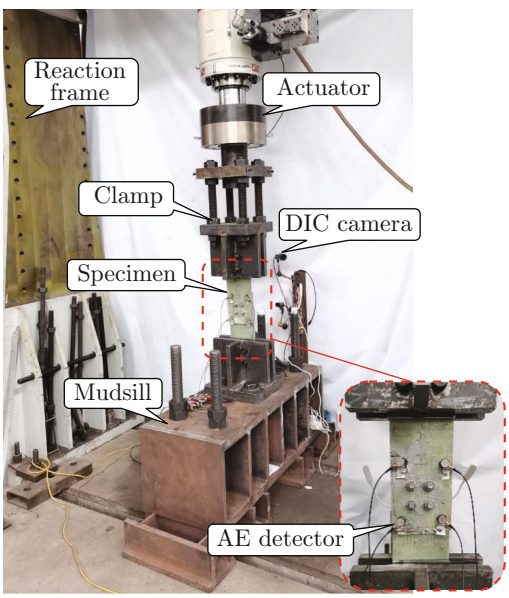

Fig. 3 Test rigs

and lower tensile clamps fastened by bolts. The cyclic load is applied with the vertical displacement of the fatigue actuator, leading to a cyclic tensile force acting on the tested specimens.

2.2 Nondestructive Measurements

The AE detectors are employed in the study to monitor the whole fatigue failure process of the specimens, as the damage of the adhesive layer can be reflected by the recorded acoustic emission signals. The AE is the transient elastic waves emitted from the material due to the rapid release of energy as the material is externally excited. A sampling frequency of 1 MHz is adopted for the AE recording in the current test campaign, and the preamplifier gain is set to be 34 dB. For each specimen, four AE detectors are arranged on the outer surface in the overlapping region as shown in Fig. 3, and each detector is attached with an L-shape support. The distance between the center of detector and the edge of the overlapping region is 20 mm. The area surrounded by the four detectors covers all bolts, ensuring that the damage signals of the adhesive layer and the edge of each bolt hole can be detected. The recording of the AE signals and the loading system are synchronized so that the loading parameters match well with the AE data.

In the previous research works, the failure modes of FRP joints were mainly measured by the following methods: ① using the strain gauges to detect the surface strain and the initial position of the crack[13], ② using the X-ray to detect the internal failure of the adhesive and plates[9], ③ adopting the optical microscope to monitor the failure state of the section[16], and ④ using thermal imaging technique to visualize the surface deformation[18]. The above measuring methods have difficulties in quantificationally illustrating the distribution and development of damages during the fatigue loading. The AE technique used in this study has the ability to monitor and illustrate the variation process of damages in the joints during the fatigue test. Additionally, the adopted 3D-DIC non-contact measurement method can precisely record the deformations, which has rarely been used in the previous studies. Compared with the previous studies, the presented research establishes a novel monitoring system for detecting the joint damages, providing a referable measuring strategy for the laboratorial fatigue test.

2.3 Fatigue Data Measurement

The fatigue life and stiffness degradation of the test specimens are recorded during fatigue loading tests. The fatigue life of the specimens is divided into two stages, which are the fatigue life corresponding to the complete failure of the adhesive layer (i.e., N_1), and the fatigue life corresponding to the complete failure of the GFRP joint (i.e., N_2). The fatigue life of the adhesive layer is defined as the loading cycles corresponding to the occurrence of apparent separation between the lapping plates, while the whole fatigue life of the GFRP joint is reached when the test specimens have been completely failed under the cyclic loading. The vertical displacement of the actuator is automatically recorded by the fatigue loading system, which is used to evaluate the stiffness degradation of the test specimens as the cyclic loading progresses. Additionally, the real-time loading cycle is denoted by n.

2.4 Loading Scheme

Before fatigue loading, static test is first conducted by using the first specimen of each group, in which the specimen will be statically loaded until failure. The corresponding failure mode and ultimate load can be obtained, which provides a reference for determining the fatigue load amplitude for the rest two specimens in each group. The static loading is controlled by displacement, and the loading rate is set to be 1 mm/min. It is found in the static test that the strength corresponding to the failure of adhesive layer is significantly less than that of the failure of bolted connection. Due to the relatively large difference between the bearing strength values of the two failure stages, different loading amplitudes are adopted for the two stages in the fatigue tests. In the first loading stage, a low load amplitude is applied until the adhesive layer has been failed. After that, the load amplitude will be increased for the second loading stage corresponding to the bolted connection failure, and the loading will finish until the GFRP joint is completely damaged. The applied fatigue load ranges for the fatigue test specimens are determined based on the corresponding failure strengths in the static loading, which are listed in Table 4, and the loading frequency is set equal to 3 Hz. Herein, $P_{\mathrm{f,a}}$ and $P_{\mathrm{f,f}}$ represent the static strength of joints corresponding to the adhesive failure and the bolted connection failure, respectively; $P_{\mathrm{min,a}}$ and $P_{\mathrm{max,a}}$ are respectively the minimum and maximum values of cyclic load in the first stage of fatigue loading (i.e., the adhesive failure); $P_{\mathrm{min,f}}$ and $P_{\mathrm{max,f}}$ denote the minimum and maximum values of cyclic load in the second stage of fatigue loading (i.e., the bolted connection failure). It is worth noting that, the first stage corresponds to the adhesive loading stage, which would end as the adhesive layer has completely damaged and lost the bearing capacity (i.e., the bonded failure). After that, the loading enters to the second stage in which the applied load is transferred to be borne by the bolts. At this stage, the joint performs mostly like a bolted connection and results in a bolted failure in the final state. The transition between the loading stages can be recognized during the loading process based on the AE signals and the loading curves.

Due to the different strength of plies at different angles in the tensile direction, in order to avoid premature failure of the weaker plies, the peak load at the GFRP loading stage was set to be less than 50%

Table 4 Static strength and fatigue life of specimens

Specimen	Static		Fatigue					
			Adhesive (bonded)			GFRP (bolted)		
	$P_{\mathrm{f,a}}$/kN	$P_{\mathrm{f,f}}$/kN	$P_{\mathrm{min,a}}$/ kN	$P_{\mathrm{max,a}}$/kN	N_1	$P_{\mathrm{min,f}}$/kN	$P_{\mathrm{max,f}}$/kN	N_2-N_1
HT1-1	62	100	—	—	—	—	—	—
HT1-2	—	—	4.8	48	—	4.8	48	150
HT1-3	—	—	2.2	22	8 339	3	30	226 609
HT4-1	60	270	—	—	—	—	—	—
HT4-2	—	—	4	40	31 303	5.8	58	136 949
HT4-3	—	—	5.8	58	21 827	52	122	85 488
HT9-1	130	460	—	—	—	—	—	—
HT9-2	—	—	8	58	275 230	40	210	3 152
HT9-3	—	—	54	124	157 541	90	160	44 052

of the GFRP static strength. In addition, due to the limited number of test specimens, different fatigue load amplitudes are selected for the two loading stages of each group of joints to obtain the corresponding fatigue life. For single-bolt joints, the fatigue load ratio R (defined as the ratio of the minimum to the maximum of the cyclic load) is set to be 0.1, and the fatigue performance of joints under different load amplitudes will be compared. For four-bolt joints, the fatigue load ratio R of specimen HT4-2 is set as 0.1 for both loading stages, and the cyclic load of the adhesive failure stage of HT4-3 is designed the same as that of the second failure stage of HT4-2, so as to compare the fatigue performance of adhesive failure stage under different load amplitudes, and investigate the difference between the adhesive failure stage and the bolt failure stage under the same cyclic load. For the nine-bolt specimen, the fatigue load amplitude of HT9-2 is taken as a relatively small value in the adhesive layer loading stage to obtain more detection data of adhesive layer. At the same time, the load amplitude in the GFRP stage is taken as a larger value to avoid being unable to obtain the final failure mode due to too long loading time. The fatigue load amplitude of HT9-3 is set to be the same as that of the four-bolt specimen HT4-3, studying the effect of bolt number on the joint's fatigue performance. The fatigue life N_1 of HT1-2 is not available since the adhesive layer of HT1-2 failed imitatively when the fatigue loads were applied. It is because the fatigue loading will have a sudden change which will lead to an overload at the initial loading while the strength of the adhesive layer is relative small. The value of N_2-N_1 for HT1-2 is smaller compared with the other specimens, which is probably because the load amplitude of HT1-2 is relatively large compared with HT1-3. Moreover, the load values of HT1-2 are relatively small compared with the loading range of the test rig ($\pm$500 kN), which leads to the problem of excessive transient load at the beginning of loading and thus the fast failure of HT1-2. In the adhesive layer loading stage, when there is a sudden change in displacement, acoustic emission signal, or obvious separation between node plates is observed; it is considered that the adhesive layer is completely damaged and the GFRP loading stage is entered.

3 Results and Discussion

3.1 Static Load-Displacement Curves

The load-displacement curves of the specimens under static tension loading of the specimens with different numbers of bolts are shown in Fig. 4. It can be seen that the variation features of the curves of the three joints are relatively similar. Once the tensile loads reach the bearing capacity of joints, the failures occur suddenly as a rapid drop can be seen in the curves after reaching the maximum load values. Additionally, there is a noticeable drop of load during the loading process for each curve, which is caused by the complete destruction of the adhesive layer. To be specific, as the bonded connection is completely damaged, the adhesive layer will no longer bear the load and a sudden increase of displacement will occur due to the gap between the hole walls and the screw, which leads to a drop in the tensile

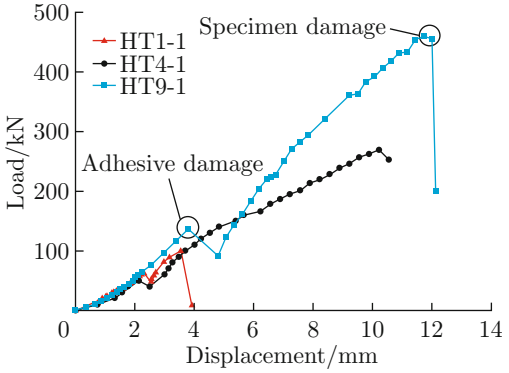

Fig. 4 Static load-displacement curves of specimens

load. Since the hole walls contact with the screw, the bolts begin to resist shear forces and the applied load can further increase. The slope of the curve (i.e., the stiffness of the specimen) after the failure of the adhesive layer drops compared with that before the failure.

The adhesive failure and ultimate failure loads of the three types of specimens are given in Table 4 and Fig. 5.

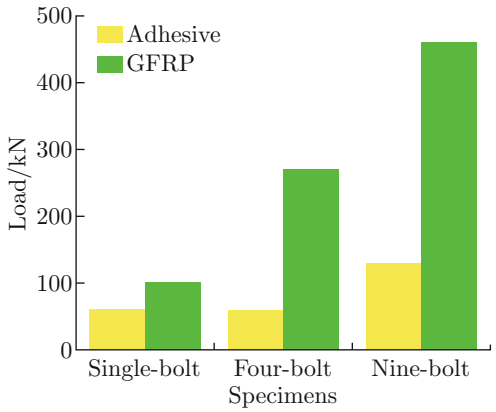

Fig. 5 Static failure loads of specimens

It is observed that the adhesive failure strength would become greater as the number of bolts increases, which is due to the greater preload between the lap plates provided by the bolts. The greater preload in the thickness direction, on the one hand, can mitigate the damage of the adhesive layer; on the other hand, it can enhance the static friction between the GFRP plates, which is beneficial for increasing the adhesive bearing strength. The ultimate bearing capacity of the nine-bolt and four-bolt specimens is 4.6 and 2.7 times higher than that of the single-bolt specimen, respectively, which can be interpreted by the fact that the shear forces beared by each bolt would be smaller for the joint with more bolts.

3.2 Progressive Fatigue Damage of Adhesive

Based on the recorded AE signals, the damage processes of the adhesive layer during the first stage of fatigue loading are shown in Figs. 6—8, respectively for one-bolt, four-bolt and nine-bolt specimens. In the figures, the x and y axes are respectively perpendicular and parallel to the tensile loading direction, and the small black points represent the AE signals corresponding to the damage locations. For the joint specimens, the initial damage of adhesive (at $0.1N_1$) occurs mainly

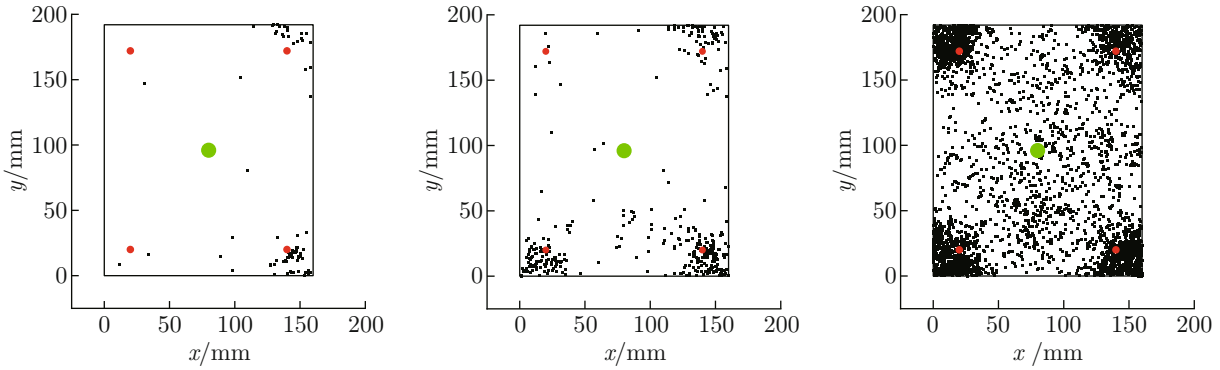

(a) Initiation ($0.1N_1$) (b) Development ($0.5N_1$) (c) Failure (N_1)

· Signal location, • Detector location, ● Bolt location

Fig. 6 Damage distribution in the adhesive layer of single-bolt specimen (HT1-2)

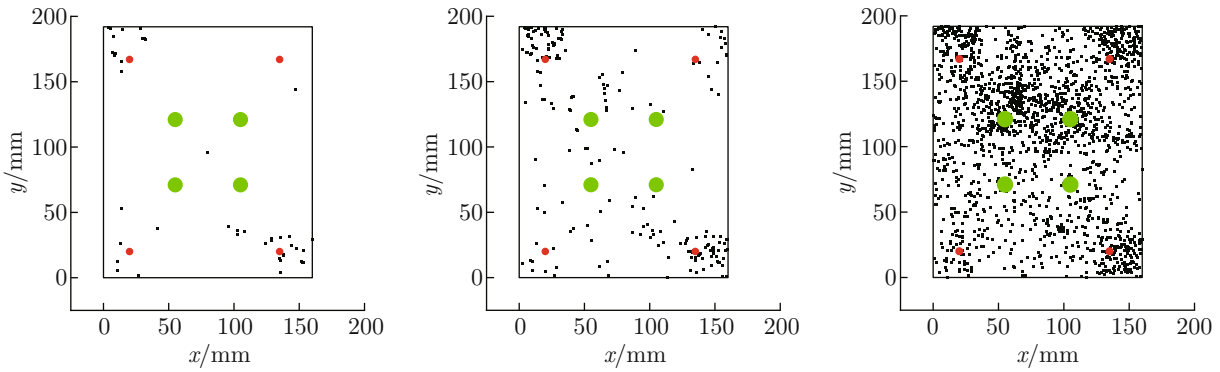

(a) Initiation ($0.1N_1$) (b) Development ($0.5N_1$) (c) Failure (N_1)

· Signal location, • Detector location, ● Bolt location

Fig. 7 Damage distribution in the adhesive layer of four-bolt specimen (HT4-2)

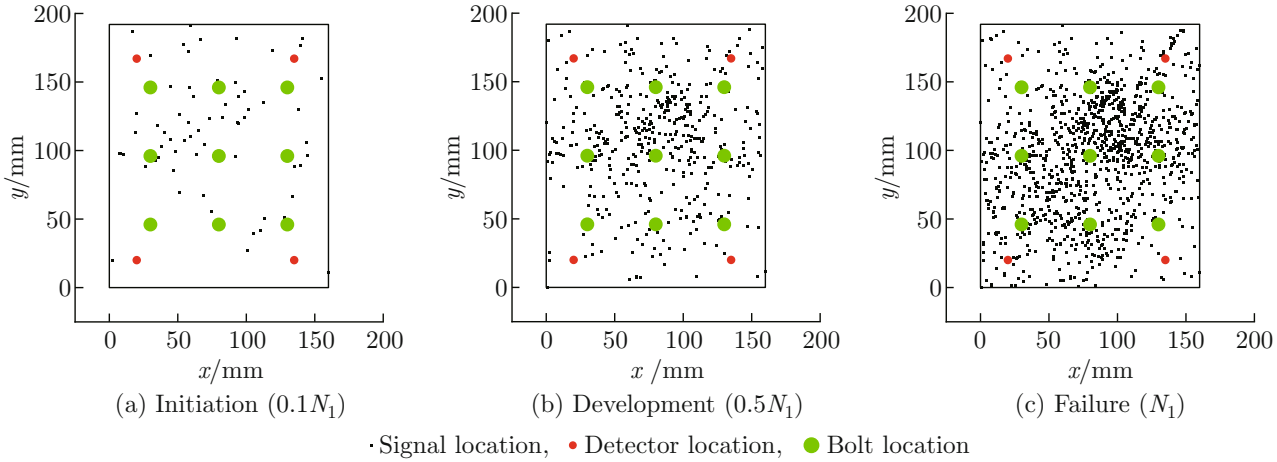

Fig. 8 Damage distribution in the adhesive layer of nine-bolt specimen (HT9-2)

at the corner of the rectangular adhesive area. Then, the damage developed gradually inward; however, it should be mentioned that the central part of the adhesive area is less damaged due to the preload effect provided by bolts. As the adhesive layer is completely damaged, the damage signals distribute all over the adhesive area with the most severe damage occurring at the corners. The detailed damage processes of the three types of joint are observed as follows:

(1) For the single-bolt specimens, the fatigue cracks first occur at the corners of the upper end of the adhesive area, and with increasing the load cycles, the fatigue cracks appear near the lower end of the adhesive area. After that, the cracks at both ends propagated gradually inward and finally gather in the center of the overlapping area. During this process, apparent separation between the two bended GFRP plates can be observed.

(2) Regarding the four-bolt specimens, the fatigue cracks of the adhesive layer also appear first at the upper end of the lapping area, and then extend quickly to the middle region of the adhesive layer. It is noticed that the crack growth rate decreased when the crack propagated near the bolt area, which can be attributed to the pressures induced by bolts. At this time, obvious bending deformation and the separation between GFRP plates in the overlapping area can be found. A loud noise can be heard when the adhesive layer is fully damaged.

(3) For the nine-bolt specimens, the fatigue cracks also present first at both ends of the adhesive layer, and further extend to the middle of the overlapping area. Like the situation of four-bolt specimens, the crack propagation rate is also found to be decreased as the cracks develop near the bolts. Considering that the adhesive layer has completely failed when the cracks extended through the adhesive area, there is no apparent separation between the two GFRP plates.

Figure 9 further presents the relationship between the number of adhesive damage points (which is detected by AE during fatigue loading process) and the fatigue load cycles, where D_n and D_{N_1} are the number of adhesive damage point corresponding to the load cycle n and N_1 respectively. From the figure it can be seen that, the damage points, to some extent, increase linearly as the loading process goes forwards, indicating that the damages develop steadily during the adhesive failure stage. Fluctuations can be seen in the curves in the middle period of the loading ($0.3N_1$ to $0.7N_1$), which is correlated with the dispersions induced by the fabrication flaws in the specimens.

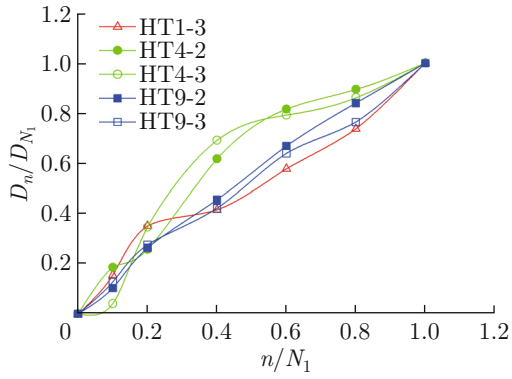

Fig. 9 Variation of adhesive damage with the loading cycles

3.3 Fatigue Failure Modes

Like the static failure process, the fatigue failure of GFRP hybrid joints can also be divided into two stages, which are the adhesive layer failure and the GFRP bolted plate failure.

Figure 10 illustrates the typical fatigue failure modes of the test specimens, in which the DIC measurement results are also provided. From the final failed specimens, it can be apparently observed that the adhesive layers have been thoroughly damaged. The fatigue

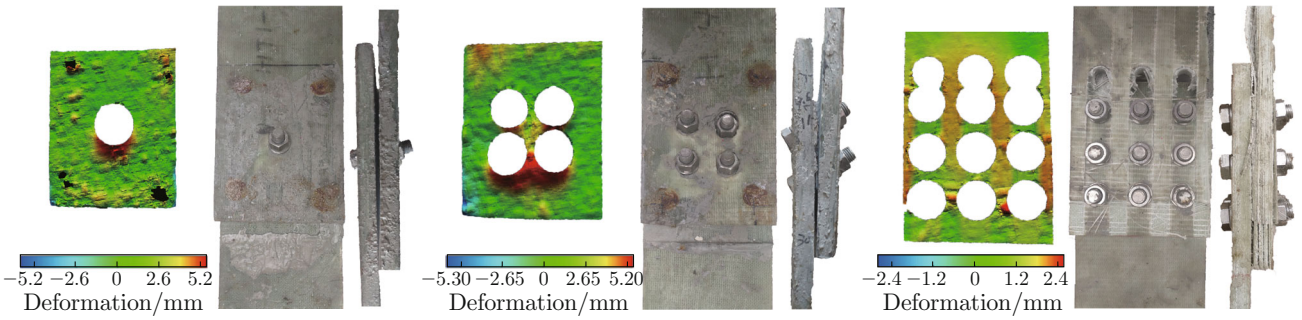

(a) Single-bolt (b) Four-bolt (c) Nine-bolt

Fig. 10 Fatigue failure modes and maximum out-of-plane deformation of specimens

cracks of the adhesive layer initiate at the upper and lower ends of the bonding area and extend to the center region. The adhesive layer will be fully damaged and invalid once the cracks initiated at the upper and lower ends intersect. After that, the external load is entirely resisted by the bolted connection, which will eventually lead to extrusion failure of the GFRP plate at the bolt holes, as well as the overall inclination of the bolts. It should be noted that the most severe damage occurs at the bolts close to the loading end (i.e., the upper end of the specimen). Due to the eccentric load of single-lap joint, out-of-plane bending deformation of different degrees can be seen for the GFRP plates in the failure joints. The final failure modes are found different for the specimens of the three groups (i.e., specimens with different bolt numbers). Specifically, the single-bolt and four-bolt specimens fail mainly with the bolt extrusion near the bolt holes, while for the case of nine-bolt specimens, the failure mode combines the tensile and delamination damages of the GFRP plates, as well as the shear failure of GFRP at the bolt holes. In the failed nine-bolt specimens, the bolt inclination is much more insignificant than those found in the single-bolt and four-bolt specimens. The DIC results indicate that the local maximum out-of-plane deformation of the GFRP plate in the nine-bolt specimens is 2.4 mm, which is remarkably smaller than that of the single-bolt and four-bolt specimens whose maximum out-of-plane deflections are respectively 5.2 mm and 5.3 mm.

3.4 AE Parameters Analysis

The characteristic parameters of acoustic emission include the energy, ring count, frequency, amplitude, duration, and rise time[22], which can reflect the damage situation of the monitored materials. In the current study, the damage propagation of the hybrid GFRP joints is analyzed based on the parameters of energy, ring count, and peak frequency.

The mentioned energy parameter of AE measurement means the elastic energy released by the acoustic emission events and its value is equal to the area enclosed by the waveform curve and coordinate axis. The energy indicates the intensity of the AE signal and is hardly affected by a threshold or the propagation characteristics. It can be used to distinguish the type of wave sources, defined as follows:

$$E_j = \int_{t_0}^{t_1} V_j(t)^2 \mathrm{d}t, \tag{1}$$

where, j denotes the channel for the recorded acoustic emission voltage $V(t)$; t_0 and t_1 are the time corresponding to the start and end of the voltage recording.

Ring counts refer to the number of oscillations exceeding a threshold. It can be used to evaluate the activity of acoustic emission, which simply reflects the strength of continuous and sudden signals. The frequency refers to the peak frequency value corresponding to the maximum value of a pulse wave, representing the frequency of the harmonic wave component with the most vital energy among all the simple harmonic members of the pulse wave. The peak frequency can characterize different types of damage of the FRP materials. Generally, the low- and medium-frequency signals correspond to the damages of matrix cracking and delamination, respectively, while the high-frequency signals correspond to fiber fracture and extraction[23].

The variations of these three parameters (i.e., energy, ring count, and peak frequency) with the load cycles are given in Figs. 11—13, where the damage development process of the specimens can be roughly divided into the following four stages:

(1) Stage I: steady development of adhesive damage. In this stage, the displacement increases slowly; in addition, the developments of the energy and ring count are quite stable. The energy values concentrate in a range of (0—1)$\times 10^8$ eu (1 eu = 1 ms $\times$ 1 mV), while the ring counts ranges from 0 to 5×10^5, which actually are all at a low level. Some specimens show the sudden displacement change, high energy and ring count at the beginning of loading, which is due to the gap between the fixture and the specimens that are clamped since loaded, and thus a noise signal has been produced. At this stage, the range of frequency is 90—160 kHz, and

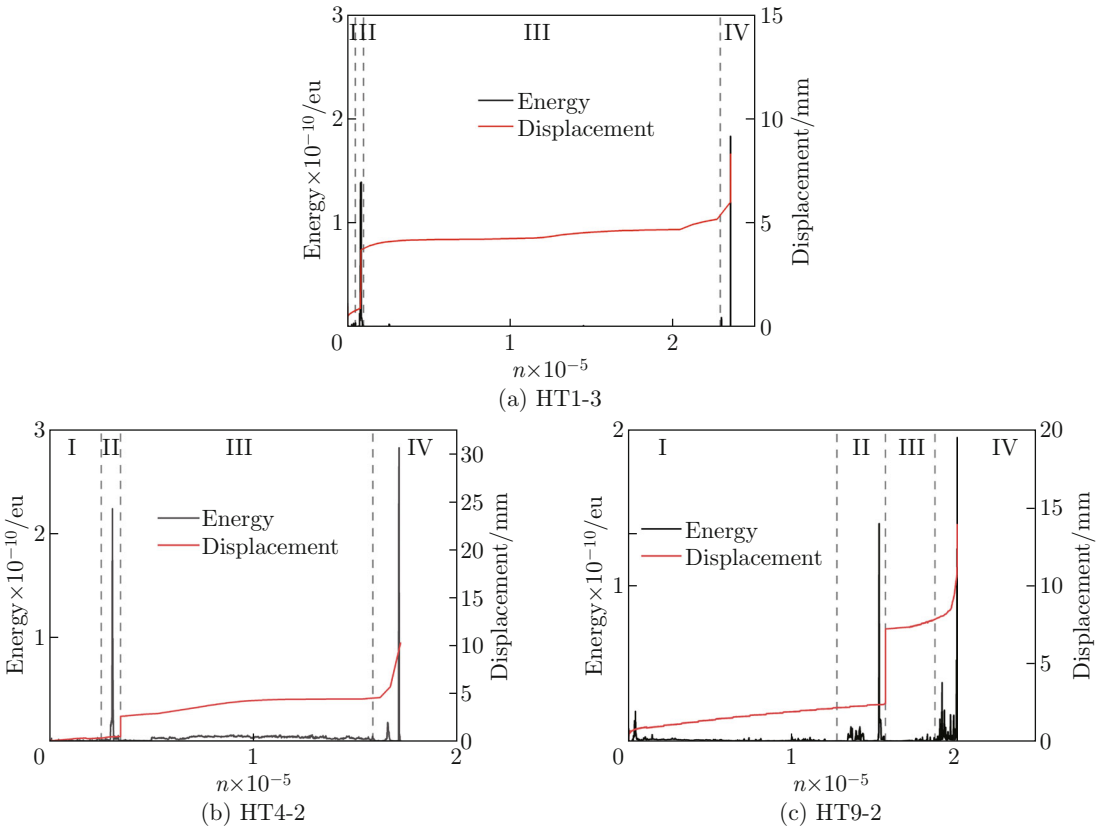

(a) HT1-3

(b) HT4-2

(c) HT9-2

Fig. 11 Variation of energy with load cycles

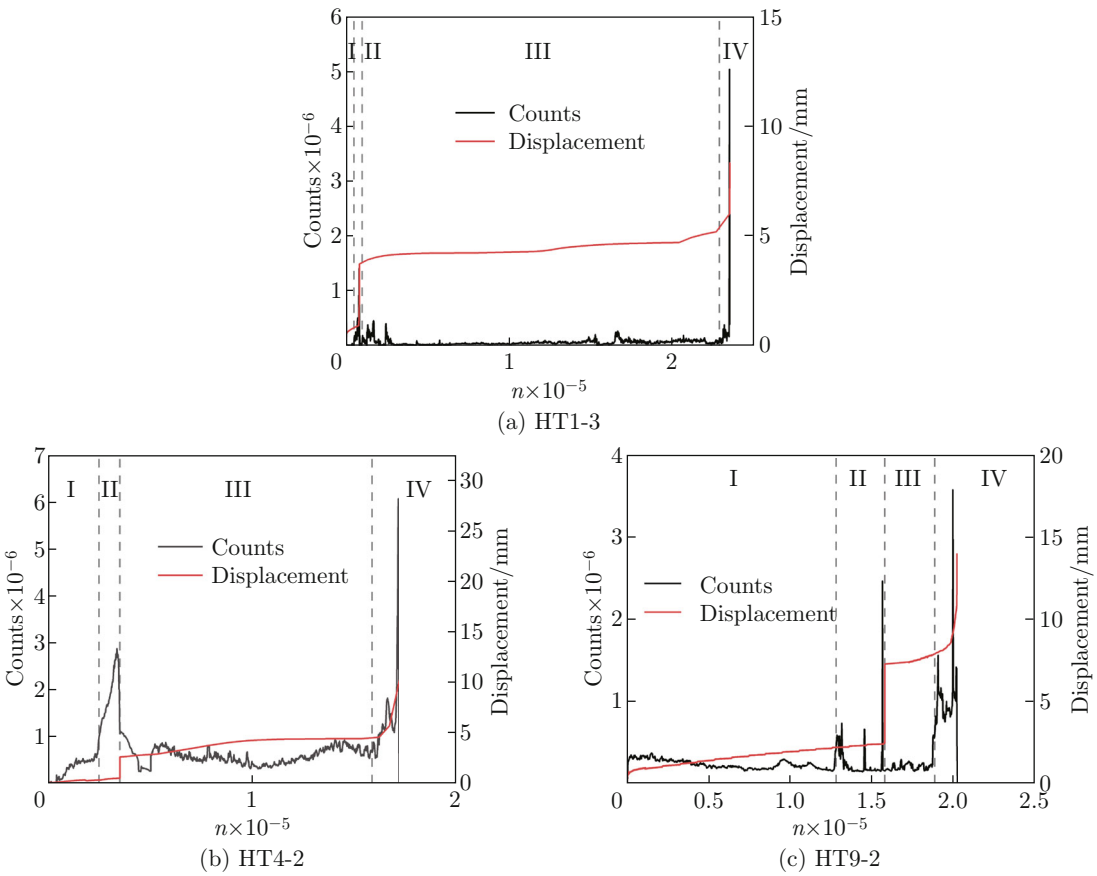

(a) HT1-3

(b) HT4-2

(c) HT9-2

Fig. 12 Variation of ring count with load cycles

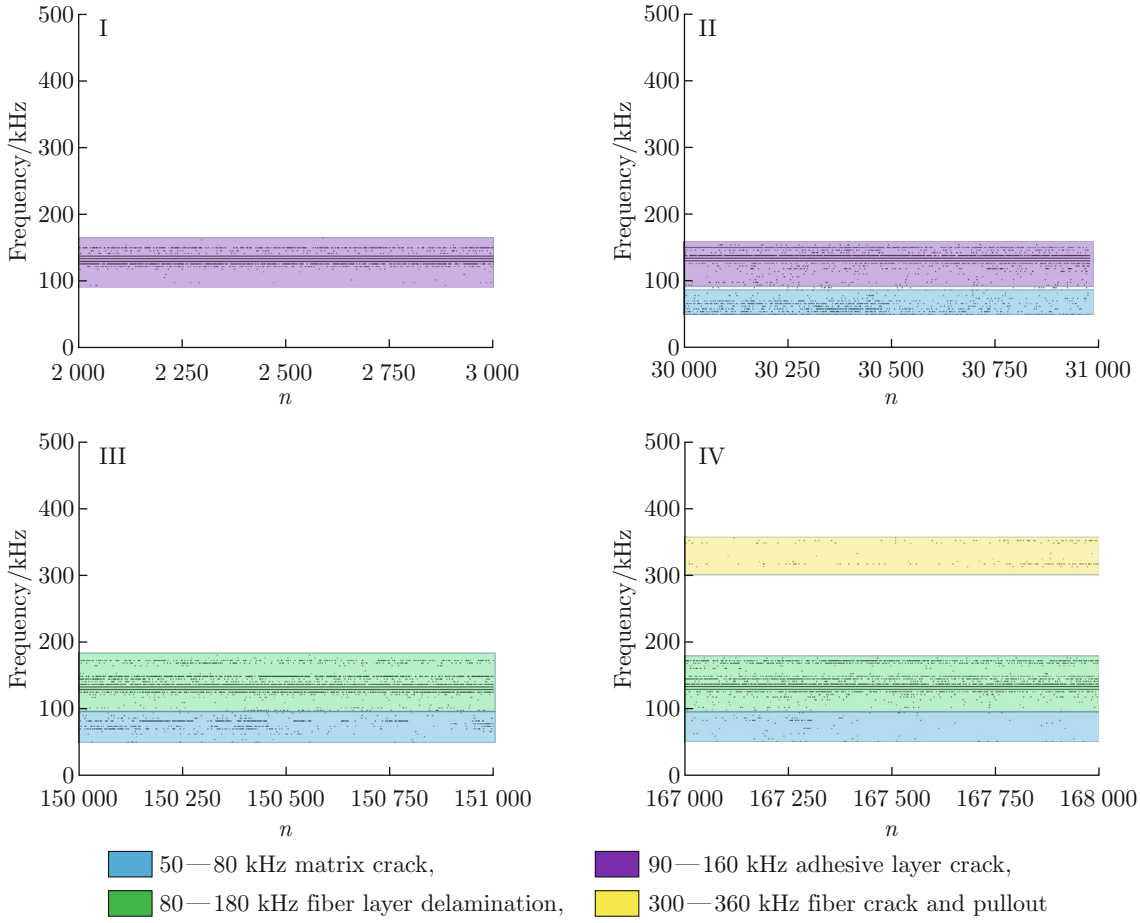

Fig. 13 Variation of frequency with load cycles (HT4-2)

few high-frequency signals can be seen. Therefore, it can be concluded that the main damage within this stage is the adhesive layer fatigue cracking.

(2) Stage II: rapid development of the adhesive damage. The energy and ring counts increase rapidly in this stage and their values are significantly higher than those in Stage I. The peak values of the energy locate in a range of $(2—3)\times10^{10}$ eu, while the ring counts are concentrated in $(2—4)\times10^{6}$. The duration of Stage II is quite short compared with Stage I since the adhesive damage develops rapidly before it has been completely cracked. In addition to the original frequency band, the frequency signals of 50—80 kHz have increased as the matrix damages of GFRP material start to be matured in this stage.

(3) Stage III: steady progressing of GFRP damage. As the adhesive layer has been completely damaged, the fatigue load amplitude is adjusted, resulting in a sudden change in the specimen's displacement (red line in Fig. 12). After that, the specimen enters a stage of steady development of the GFRP damage, and the displacement increases slowly. Meanwhile, the values of the energy and count are similar to those of Stage I. In this stage, the energy values locate in a range of $(0—1)\times10^{9}$ eu, and the ring counts are concentrated in $(0—1)\times10^{6}$, which are slightly higher than the values in Stage I. The values of the signal frequency are within ranges of 50—80 kHz and 80—200 kHz, which are respectively regarded as the low-frequency and medium-frequency ranges. The corresponding damage types in this frequency ranges are matrix cracking and delamination.

(4) Stage IV: rapid development of GFRP damage. In this stage, the displacements increase quickly and the joint specimens are gradually destroyed. The growth rates of energy and ring count are accelerated and the corresponding curves finally reach the peak values when the joints are completely failed. The energy peaks are concentrated in $(1—3)\times10^{10}$ eu and the ring counts locate in a range of $(3.5—6)\times10^{6}$. In this stage, the frequencies are found in all the low-, medium-, and high-frequency ranges, which are 50—80 kHz, 80—200 kHz, and 300—360 kHz, respectively. The corresponding damage types include matrix cracking, delamination, fiber fracture, and fiber pulling.

The ranges of the acoustic emission characteristic parameters and the corresponding damage types of joint specimens in the aforementioned four stages are further

Table 5 AE characteristic parameters

Stage	Energy/eu	Ring count	Frequency/kHz	Failure mode
I	(0—1) × 10^8	(0—5) × 10^5	90—160	Adhesive crack
II	(2—3) × 10^{10}	(2—4) × 10^6	50—80, 80—180	Matrix crack and adhesive crack
III	(0—1) × 10^9	(0—1) × 10^6	50—80, 80—200	Matrix crack and fiber layer's delamination
IV	(3—4) × 10^{10}	(2—6) × 10^6	50—80, 120—180, 300—360	Matrix crack, fiber layer's delamination, fiber crack, and pullout

3.5 Stiffness Degradation

To investigate the stiffness degradation of the test specimens during fatigue loading and its relationship with the final failure mode, the correlation curves between the vertical displacement of test specimens and the number of load cycles are analyzed and shown in Fig. 14. Since the variation of the specimen stiffness before the adhesive failure is insignificant, the normalized load cycle in Fig. 14 is defined as $(n - N_1)/(N_2 - N_1)$, that is, the ratio of the actual loading cycles after the adhesive failure to the fatigue life after the adhesive failure. The normalized displacement is expressed as the ratio of the initial vertical displacement d_0 to the current vertical displacement d.

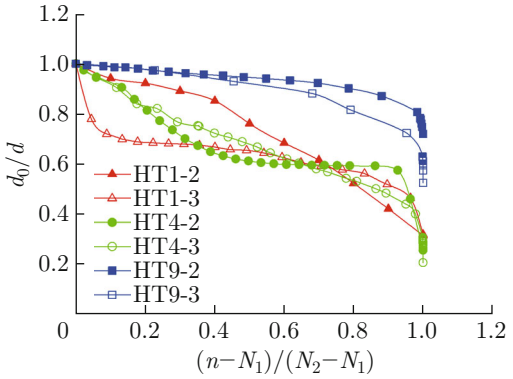

Fig. 14 Stiffness degradation of specimens

As can be found from Fig. 14, the vertical displacements of the test specimens increase steadily in the whole loading process, and as reaching the final failure, the displacements increase sharply. The number of bolts shows an obvious effect on the stiffness degradation of specimens. Specifically, the stiffness degradation of nine-bolt specimens is relatively moderate at the early fatigue loading, and becomes faster near the final fatigue failure. However, the stiffness of single-bolt and four-bolt specimens decreased rapidly throughout the fatigue loading, especially for the single-bolt specimen, significant degradation may occur soon after the adhesive failure. The stiffness degradation of nine-bolt specimens near failure is calculated to be 15%—20%, while those of single-bolt and four-bolt specimens are greater than 40%. The results indicated that the increasing number of bolts can effectively improve the performance of GFRP hybrid joint's stiffness degradation resistance.

3.6 Fatigue Life

It can be seen in Table 4 that the fatigue life of specimen HT1-2 in the second loading stage (i.e., $N_2 - N_1$) is relatively small compared with those of other specimens, which can be interpreted regarding the load resisted by the single bolt, and the constraint on the plates provided by the single bolt. First, compared with the bolts in the four- or nine-bolt specimens, the single bolt of specimen HT1-2 bears a relatively high load during the fatigue loading, which can lead to a more significant local damage in the GFRP plates. On the other hand, for the second fatigue loading stage of the single-bolt specimens, since the unique bolt can provide limited constraint to the connected GFRP plates, and that the cyclic loading is controlled by load but not displacement, it is found during the loading process that as the specimens approach to failure, the displacement can be relatively large, which would cause a significant dynamic impact on the hole wall of GFRP plates, leading to an acceleration of damage in the GFRP material. This phenomenon was found more severe in the specimens HT1-2 than HT1-3, since the load amplitude and the maximum value of the cyclic load for HT1-2 are quite greater than those of the HT1-3.

For the same type of joints, the smaller the fatigue load amplitude is, the greater the fatigue life of each loading stage will be. Except for the nine-bolt joints, the fatigue life of the bolted connection is higher than that of the bonded connection even if the fatigue load amplitudes used in bolted connection failure stage are greater. This may be because the nine-bolt specimens have an excellent integrity so that the bolted connection has worked together with the bonded connection during the adhesive layer failure stage.

Under the condition of higher fatigue load amplitude, for the joints with more bolts, the fatigue life of the bonded connection will be higher, and so does the final fatigue life of the joints. By comparing the nine-bolt specimen (HT9-3) with the four-bolt specimen (HT4-3), it can be found that under the same load amplitude, the fatigue life of the bonded connection of the nine-bolt specimen is higher than the overall fatigue life of

the four-bolt specimen. However, the fatigue life of the bolted connection of nine-bolt specimen is lower than that of the four-bolt specimen, which shows again that the bolted connection of nine-bolt specimen has involved in the previous loading stages.

Since there is lack of the S-N fatigue design curves of the single-lap GFRP hybrid joint in the existing specifications, based on the test results, the relevant S-N curves are proposed in this section, as presented in Fig. 15. In the figure, the test data are marked by the points representing the relationship between the fatigue stress S and the fatigue life N of the test specimens under tensile loading condition. Herein, the tensile stress is calculated by $S = F_{\mathrm{r}}/(wb)$, where F_{r} is the fatigue load range amplitude, and w and b are the width and thickness of the GFRP plate, respectively. Since the fatigue stress amplitudes before and after the adhesive layer failure are different, in order to properly consider the adhesive fatigue life N_1 in the proposed S-N curves, it is equivalent to a fatigue life N_1', with which the equivalent overall fatigue life of the GFRP hybrid joints in the S-N curves can be calculated as $N = N_2 - N_1 + N_1'$. For each group of specimens, N_1' is obtained by an extrapolation based on the fatigue test data. For each specimen group, the linear relationship between N_1 and S is determined based on results of the two fatigue-load specimens, and then, the equivalent fatigue life N_1' of the adhesive failure stage is determined as the value of N_1 corresponding to the enlarged stress amplitude S in the following GFRP failure stage, based on the abovementioned linear relationship.

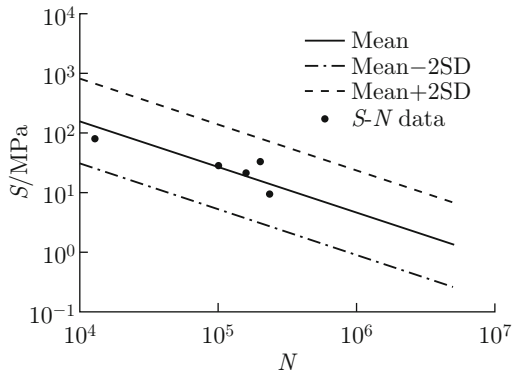

Fig. 15 Fatigue S-N curves of specimens

The least square method is used for fitting the S-N curves in this study, and the curve expression is as follows:

$$\lg N = A + B \lg S - 2\sigma_{\lg N}, \tag{2}$$

where, A and B are the data fitting parameters; $\sigma_{\lg N}$ is the standard deviation of lg N. The lower bound equation with 95% confidence is used as the S-N design curve. In Fig. 15, three types of fitting curves are provided, which respectively are: Mean; Mean+2SD; Mean-2SD, where the SD is the standard deviation.

Based on the fitting analysis, the mean curves of the fatigue life of the GFRP hybrid joints are obtained as follows:

$$\lg N = 5.944 - 1.303 \lg S, \tag{3}$$

Limited by the test data, the constructed S-N curve model ignores the influence of bolt size, bolt spacing, GFRP plate thickness, fiber ply, and so on. However, the presented curves can provide a reference for the fatigue design of the single-lap GFRP hybrid bonded/bolted joints.

4 Conclusion

In this paper, the static and fatigue performance of the GFRP hybrid bonded/bolted joints under tensile loading condition has been experimentally investigated. Based on the test results, the following main conclusions can be drawn:

(1) For static loading, the variation trends of load with the displacement of different types of specimens are similar. The ductility of the adhesive layer and the overall stiffness would increase for the joints with more bolts. The static strength of GFRP hybrid joints is dominated by the bolted connection. For the nine-bolt specimens, the ultimate strength of the bolted connection is about 3.5 times of the strength corresponding to the adhesive failure.

(2) The fatigue failure process of the GFRP hybrid joints can be divided into four stages, which are: ① cumulative damage of adhesive layer, ② damage of the adhesive layer, ③ cumulative damage of GFRP plate, and ④ damage of GFRP plate. The AE characteristic parameters can be used to recognize the occurrence of failure, as the parameter values corresponding to the adhesive failure stage and the GFRP failure stage would change significantly. For the joints with few bolts, the final failure mode is shown to be extrusion failure at the bolt holes. The fiber tensile and shear failures would occur as more bolts are used for the joints.

(3) The stiffness degradation of nine-bolt specimens is relatively moderate at the early fatigue loading, and becomes faster near the final fatigue failure. For single-bolt and four-bolt specimens, the stiffness decreased rapidly throughout the fatigue loading. The total degradations of the nine-bolt specimens are read to be 15%—20%, while it is found to be greater than 40% for single- and four-bolt specimens. The increasing number of bolts can effectively improve the performance of GFRP hybrid joint's stiffness degradation resistance.

(4) The fatigue life corresponding to the adhesive failure and bolted connection failure can be improved with increasing the bolt number. For the joint with more

bolts (e.g., the nine-bolt specimen in this study), the bolted connection has participated in the load bearing before adhesive failure, due to which the fatigue life of bolted connection failure is lower than the that of adhesive failure for such joints. Based on the fitting analysis with test data, the S-N curves for the single-lap GFRP hybrid bonded/bolted joints under tensile loading condition are proposed, which provide a reference for the fatigue life design of such type of joint.

References

[1] ZAMAN A, GUTUB S A, WAFA M A. A review on FRP composites applications and durability concerns in the construction sector [J]. *Journal of Reinforced Plastics and Composites*, 2013, **32**(24): 1966-1988.

[2] MCCARTHY M A, LAWLOR V P, STANLEY W F, et al. Bolt-hole clearance effects and strength criteria in single-bolt, single-lap, composite bolted joints [J]. *Composites Science and Technology*, 2002, **62**(10/11): 1415-1431.

[3] MCCARTHY M A, LAWLOR V P, STANLEY W F. An experimental study of bolt-hole clearance effects in single-lap, multibolt composite joints [J]. *Journal of Composite Materials*, 2005, **39**(9): 799-825.

[4] SUN H T, CHANG F K, QING X L. The response of composite joints with bolt-clamping loads, part I: Model development [J]. *Journal of Composite Materials*, 2002, **36**(1): 47-67.

[5] SUN H T, CHANG F K, QING X L. The response of composite joints with bolt-clamping loads, part II: Model verification [J]. *Journal of Composite Materials*, 2002, **36**(1): 69-92.

[6] KHASHABA U A, SALLAM H E M, AL-SHORBAGY A E, et al. Effect of washer size and tightening torque on the performance of bolted joints in composite structures [J]. *Composite Structures*, 2006, **73**(3): 310-317.

[7] SEN F, PAKDIL M, SAYMAN O, et al. Experimental failure analysis of mechanically fastened joints with clearance in composite laminates under preload [J]. *Materials & Design*, 2008, **29**(6): 1159-1169.

[8] DE IORIO A, LECCE L, MIGNOSI S. Fatigue damage evaluation in multifastened CFRP joints [M]//Proceedings of the 6th International Conference on Fracture. Amsterdam: Elsevier, 1984: 3045-3051.

[9] HERRINGTON P D, SABBAGHIAN M. Fatigue failure of composite bolted joints [J]. *Journal of Composite Materials*, 1993, **27**(5): 491-512.

[10] HUANG W J, CHENG X Q, WU P F, et al. Analysis on tensile properties and influence factors of composite hybrid joints [J]. *Journal of Beijing University of Aeronautics and Astronautics*, 2013, **39**(10): 1408-1413 (in Chinese).

[11] READ P J C L, SHENOI R A. Fatigue behaviour of single skin FRP tee joints [J]. *International Journal of Fatigue*, 1999, **21**(3): 281-296.

[12] QUARESIMIN M, RICOTTA M. Life prediction of bonded joints in composite materials [J]. *International Journal of Fatigue*, 2006, **28**(10): 1166-1176.

[13] ZHANG Y, VASSILOPOULOS A P, KELLER T. Fracture of adhesively-bonded pultruded GFRP joints under constant amplitude fatigue loading [J]. *International Journal of Fatigue*, 2010, **32**(7): 979-987.

[14] KIM K S, YOO J S, YI Y M, et al. Failure mode and strength of uni-directional composite single lap bonded joints with different bonding methods [J]. *Composite Structures*, 2006, **72**(4): 477-485.

[15] SARKANI S, MICHAELOV G, KIHL D P, et al. Stochastic fatigue damage accumulation of FRP laminates and joints [J]. *Journal of Structural Engineering*, 1999, **125**(12): 1423-1431.

[16] KELLY G. Quasi-static strength and fatigue life of hybrid (bonded/bolted) composite single-lap joints [J]. *Composite Structures*, 2006, **72**(1): 119-129.

[17] HOANG-NGOC C T, PAROISSIEN E. Simulation of single-lap bonded and hybrid (bolted/bonded) joints with flexible adhesive [J]. *International Journal of Adhesion and Adhesives*, 2010, **30**(3): 117-129.

[18] CHOWDHURY N M, CHIU W K, WANG J, et al. Experimental and finite element studies of bolted, bonded and hybrid step lap joints of thick carbon fibre/epoxy panels used in aircraft structures [J]. *Composites Part B: Engineering*, 2016, **100**: 68-77.

[19] CHOWDHURY N M, WANG J, CHIU W K, et al. Static and fatigue testing bolted, bonded and hybrid step lap joints of thick carbon fibre/epoxy laminates used on aircraft structures [J]. *Composite Structures*, 2016, **142**: 96-106.

[20] RAJU K P, BODJONA K, LIM G H, et al. Improving load sharing in hybrid bonded/bolted composite joints using an interference-fit bolt [J]. *Composite Structures*, 2016, **149**: 329-338.

[21] The State Bureau of Quality and Technical Supervision. Test method for tensile properties of oriented fiber reinforced plastics: GB/T 3354-1999 [S]. Beijing: Standards Press of China, 1999 (in Chinese).

[22] MENG C, PENG W D, NING X B, et al. Investigation on the acoustic emission characteristics during the damage of glass fiber composite [J]. *Fiber Reinforced Plastics/Composites*, 2016(12): 23-27 (in Chinese).

[23] LI X, KANG Z L, XU K H, et al. Characteristics research for acoustic emission testing signal of different damage of GFRP [J]. *Journal of Nanchang Hangkong University* (*Natural Sciences*), 2016, **30**(4): 75-81 (in Chinese).